Characteristics of Numerically Simulated Mesoscale Convective Systems and Their Application to Parameterization

M. E. B. GRAY

The Met. Office, Bracknell, Berkshire, United Kingdom

(Manuscript received 14 July 1999, in final form 18 January 2000)

ABSTRACT

A cloud-resolving model simulation of a convectively active phase of the Tropical Ocean Global Atmosphere Coupled Ocean–Atmosphere Response Experiment (TOGA COARE) is used to study the properties of the convective and mesoscale updrafts, and precipitating downdrafts of the simulated mesoscale convective systems (MCSs). Analysis of scalar transports confirms the results of previous studies that show that the mesoscale updraft provides an important contribution to the total heat and moisture budget of the MCS in the upper troposphere. The mesoscale updraft is shown to possess little or no positive buoyancy, and it is suggested that the upward vertical motion present is associated with decaying convective cells. Momentum transports are not significant in the mesoscale updraft, but those in the mesoscale downdraft are of the same order as those in the convective downdraft. Horizontal mesoscale circulations, such as rear-to-front inflow, may be important in determining the downdraft momentum transport.

Using the cloud-resolving model results, a mass flux parameterization for the mesoscale updraft is proposed. The mass flux equation is closed by assuming that a fraction of the mass flux detrained from the convective cores is entrained into the mesoscale updraft. Along with a simple evaporation-based parameterization for the mesoscale downdraft, the parameterization is tested in a single-column model for the same TOGA COARE period. Comparisons of the cloud-resolving model and single-column model results show very good agreement between the simulated and parameterized mesoscale scalar transports when the parameterized convection is also well represented. The importance of an accurate convection scheme to drive the mesoscale updraft–downdraft parameterization is stressed.

1. Introduction

Mesoscale convective systems (MCSs) have been defined by Houze (1993) as cloud systems associated with thunderstorms that produce a contiguous precipitation area with a horizontal extent of 100km or more in at least one direction. They differ from single, simple multicell or discrete lines of thunderstorms in that they exhibit a substantial area of stratiform precipitation. Although the rainfall in this stratiform region is much less intense than that from the accompanying convective cells, it covers a much greater area, and so over the lifetime of the system, the stratiform rainfall may account for between a quarter and a half of the total MCS precipitation (Houze 1993). Such weather systems are important from a forecasting and climatological perspective. The former because of the severe weather associated with MCSs and the latter because MCSs are major contributors of rainfall in the Tropics and summer hemisphere continents. For example, Fritsch et al. (1986) attribute up to 70% of the warm season rainfall over the midwest United States to MCSs.

Observations of MCSs, such as those from the Global Atmospheric Research Programme (GARP) Atlantic Tropical Experiment by Zipser (1977) and Houze (1977), have shown that the dynamics of MCSs also differ from those of individual thunderstorms. In particular, system-scale circulations are observed that are on scales too great to be associated with single convective cells. Although the exact nature of these mesoscale circulations may vary between different types of MCSs, in general, a mesoscale updraft of tens of centimeters per second exists within the anvil cloud of the stratiform region, whereas a mesoscale downdraft, of the same order of magnitude, is observed beneath anvil base in the stratiform rainfall. These are in addition to the convective-scale updrafts and downdrafts associated with the convective cells.

Traditional approaches to convective parameterization have neglected these mesoscale circulations. If the grid spacing of the general circulation model (GCM) is sufficiently fine, then these circulations should be resolved and parameterization is not necessary. However, the resolution of many GCMs is still not at this level, and these additional transports in MCSs may be absent.

Corresponding author address: Dr. M. E. B. Gray, The Met. Office, London Road, Bracknell, Berkshire RG12 2SZ, United Kingdom.
E-mail: mebgray@meto.gov.uk

Johnson (1984) partitioned observed apparent convective heat sources and moisture sinks (Q_1 and Q_2, respectively) into mesoscale and convective-scale components. He showed that the mesoscale contribution to Q_1 was around $\pm$2–3 K day^{-1} per cm rainfall per day compared to a maximum value of around 5 K day^{-1} per cm rainfall per day for the convective component. Similar values were also diagnosed for the Q_2 components. The mesoscale component provides a dipole of heating and moistening; the mesoscale updraft heats and dries the atmosphere above the freezing level, while the mesoscale downdraft cools and moistens the atmosphere below.

This potential shortfall of convective parameterization schemes was addressed by Donner (1993). His scheme, which represented the vertical momentum of the convective updrafts, rather than just the mass flux, so as to be able to more accurately represent the in-cloud microphysical processes, also included a parameterization for mesoscale effects. He considered that the mesoscale updraft would affect the environment through the redistribution of moisture from the convective updrafts, in situ deposition, and eddy transports. The impacts on the environment of the mesoscale downdraft would similarly include melting, sublimation, and eddy transports. The equation set necessarily contained some assumptions of microphysical conversion rates, vertical velocity, and transports between convective and mesoscale circulations for which the study by Leary and Houze (1980) provided some values. Alexander and Cotton (1998) attempted to further refine Donner's scheme by using cloud-resolving model (CRM) simulations of a tropical and midlatitude MCS to define profiles for some of these assumed properties. However, Alexander and Cotton acknowledged that the parameterization parameters determined from their CRM experiments vary between MCSs and also over the MCS life cycle. Nevertheless, both schemes represent plausible mesoscale heating and drying dipoles. There is certainly scope for further improvements, particularly in reducing the number of disposable parameters and trying to link the properties of the mesoscale drafts more closely to those of the driving convection parameterization scheme.

The aim of this investigation is to study the properties of mesoscale updrafts and downdrafts in cloud-resolving model simulations of a westerly wind burst event from the 1992/93 Tropical Ocean Global Atmosphere Coupled Ocean–Atmosphere Response Experiment (TOGA COARE) and to use that information to help construct an alternative representation for mesoscale circulations that can be used in convective parameterization schemes. The 6-day period from 0000 UTC 20 December 1992 is selected, which has been extensively studied as part of the Global Energy and Water Cycle Experiment (GEWEX) Cloud System Study (GCSS) Working Group 4 (Moncrieff et al. 1997). This dataset covers a convectively active period in which a large number of MCSs were observed. It is hoped that this will provide an ensemble of MCSs in tropical conditions from which to derive the mean properties of the mesoscale circulations. Section 2 will describe the cloud-resolving model and experiment. The properties of the simulated MCS, including the scalar and momentum transports of the convective and mesoscale drafts, will be discussed in section 3, and these results will be used to design a parameterization to be described in section 4. This parameterization will be tested in a single-column model in section 5, and section 6 will contain some concluding remarks.

2. Cloud-resolving model experiment

a. Model formulation

The simulations are performed using the cloud-resolving model described in Shutts and Gray (1994). It solves an anelastic, quasi-Boussinesq set of equations, representing moist processes through a liquid water static energy variable, T_L, defined as

$$T_L = T + \frac{(gz - L_v r_L)}{c_p}, \tag{1}$$

where T is the temperature, g the acceleration due to gravity, z the height, L_v the latent heat of vaporization, r_L the liquid water mixing ratio, and c_p the specific heat of air at constant pressure. In the current formulation a more sophisticated microphysics package is used (Swann 1998) compared to that of Shutts and Gray (1994) including representations for cloud ice, snow, graupel, and rain. The cloud ice is modeled using a double-moment scheme, by which both mixing ratios and number concentrations are prognostically calculated, whereas the snow, graupel, and rain are modeled using single-moment schemes, which only involves the mixing ratio. A cloud-interactive long- and shortwave radiation scheme is interfaced to the model, which is based on the GCM scheme of Edwards and Slingo (1996) with additional treatments for snow, graupel, and rain. Scalar variables are advected using the ULTIMATE QUICKEST scheme of Leonard et al. (1993); momentum is advected using the centered difference scheme of Piacsek and Williams (1970). The subgrid turbulence parameterization is described in Brown et al. (1994) and is based on the Smagorinsky–Lilly model (Mason 1989) with a revised Richardson number calculation to take account of moist processes.

The simulation is conducted on a 128 $\times$ 128 $\times$ 60 grid with a grid spacing of 2 km in the horizontal. In the vertical, the grid spacing stretches from 150 m in the boundary layer to 330 m in the free troposphere and then up to 500 m at the domain top of 20 km. Periodic horizontal boundary conditions are used. The surface boundary is assumed to have a homogeneous temperature and be at saturation, with the turbulent fluxes at the surface calculated pointwise using Monin–Obukhov

similarity. The upper boundary is a rigid lid, which can lead to a spurious buildup of gravity wave energy in the domain. To alleviate this a Newtonian damping layer is introduced in the upper 5 km of the domain, which relaxes all prognostic variables back to their large-scale mean through an additional source term

$$\frac{\partial \phi}{\partial t} = -\lambda(z)(\phi - \overline{\phi}), \tag{2}$$

where $\lambda(z)$ is a height-dependent damping coefficient, ϕ is an arbitrary prognostic variable, and an overbar signifies a horizontal mean. The need for a deep damping layer, and the restriction on computing resources in performing a 3D simulation, mean that relaxation has to occur below the model tropopause (17 km). However, 2D sensitivity tests comparing this damping layer formulation with one starting at 18 km and extending up to a new domain top of 23 km show insignificant differences, so it is reasonable to assume that the subtropopause damping layer has no detrimental impact on the simulation.

b. Initial conditions

The model is initiated using profiles of temperature, humidity, and horizontal momentum measured from the TOGA COARE intensive flux array (IFA) for 0000 UTC 20 December 1992. All other model fields are initiated to zero. The temperature field in the lowest 200 m is modified by the addition of randomly generated noise of maximum amplitude 0.25 K. These perturbations are required for convective circulations to develop. The initial profile was observed prior to the onset of a convectively active westerly wind burst that led to the development of several MCSs over the subsequent 6 days (Chen et al. 1996). Large-scale advection of temperature and humidity is modeled by using forcing data taken from the IFA at 6-h intervals. These values are interpolated so as to provide a smooth forcing function in time. Large-scale horizontal momentum forcing is modeled by relaxing the momentum fields back to observations over a 3-h timescale. Observations of sea surface temperature are used to vary the model surface temperature.

c. Conditionally sampled diagnostics

In order to investigate the properties of the stratiform regions of the simulated MCSs, some criteria must be employed to identify the convective and mesoscale components of the MCS circulation. The challenge is not just to differentiate between convective and mesoscale motions but also to eliminate other motions, such as inertia–gravity waves. Two approaches are used here, both of which have some disadvantages.

The first technique is to subdivide the model domain into convective or stratiform columns depending on the surface precipitation rate, P. This strategy has been used in other studies such as Tao and Simpson (1989). The column classification criteria used here are those suggested by Steiner et al. (1995) using radar and rain gauge data near Darwin, Australia. A column is defined as convective if 1) P exceeds 10 mm h^{-1}; 2) P exceeds the background rate (the mean of all points within an 11-km radius) by a factor of 2; or 3) the column is within a specified radius, R, of a column defined as convective by criterion 1 or 2, where R is a function of P. All columns with P exceeding 0.01 mm h^{-1} that are not convective are defined as stratiform. However, as noted by Tao and Simpson (1989), such a partitioning may have its drawbacks. Convective-scale updrafts may be tilted such that at upper levels they penetrate the stratiform columns. Also, evolving convective cells at the head of the convective line can be spuriously defined as stratiform, leading to areas of ascent in the stratiform columns below the freezing level.

In an attempt to overcome some of these problems, the second conditionally sampling technique works on a pointwise basis using thresholds to define the convective and mesoscale circulations. A grid point is defined as being part of a convective updraft if the vertical velocity at that grid point exceeds 1 m s^{-1}. This is a commonly used vertical velocity threshold (e.g., Kershaw and Gregory 1997) to describe the strongest updrafts, assumed to be part of the deep convective circulation. These are shown to be reasonably consistent with the convective column updrafts for heights less than about 8 km, above which updrafts in the latter tilt into stratiform columns. Mesoscale updrafts must necessarily not exceed 1 m s^{-1} to be congruous with the definition of the convective updraft. However, a low threshold must be introduced to eliminate as much gravity wave activity as possible from the definitions. This is set at 0.25 m s^{-1}, and minimum thresholds for ice and snow mixing ratios (10^{-7} kg kg^{-1}) are also enforced in an attempt to exclude radiation-induced circulations in nonprecipitating cirrus cloud and ensure that the updraft is located in the MCS anvil above the freezing level. Although the entire gravity wave spectrum is not excluded by this definition, grid point analysis of the mesoscale updraft as defined above shows that relatively large contiguous areas of ascent are captured, suggesting that the impact of gravity waves may not be high. In the following sections references to convective updrafts and mesoscale updrafts relate to these pointwise definitions.

Precipitating downdrafts are also conditionally sampled and defined as descending air in which the sum of all precipitating hydrometeors exceeds 10^{-4} kg kg^{-1}. Precipitating downdrafts that occur in stratiform columns are taken to be mesoscale downdrafts, whereas those that occur in convective columns are assumed to be convective-scale downdrafts. This is a reasonable approximation close to the surface but, due to the tilt of the systems with height, becomes more uncertain at higher altitudes.

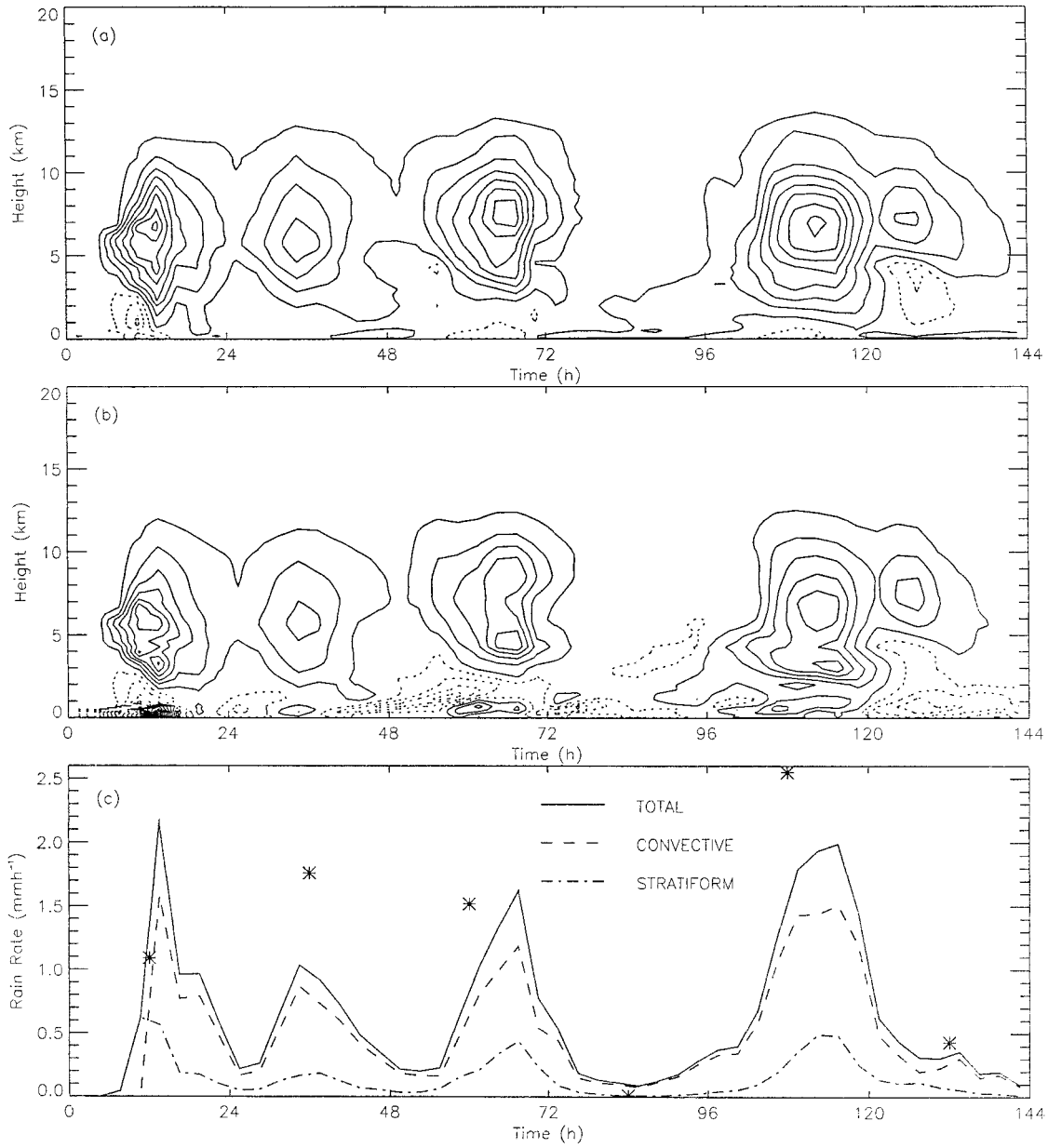

FIG. 1. Time–height profile of (a) the apparent heat source, Q_1; and (b) the apparent moisture sink, Q_2, for the 6 days of the simulation. The contour interval is 4 K day^{-1} with the first contour at 2 K day^{-1} with negative values dashed. (c) Time series of domain-average surface rainfall rate for the same period. The dashed and dash–dot lines in (c) show the convective and stratiform components of the rainfall respectively, whereas the asterisks indicate values estimated from the microwave sounding unit given in Chen et al. (1996).

3. Properties of simulated MCSs

a. Overview of simulation

Figure 1 shows time series of the domain-average apparent heat source, Q_1; domain-average apparent moisture sink, Q_2; and surface rainfall rate. These show four strong periods of convection on days 1, 2, 3, and 5 of the simulation. In Fig. 1c microwave sounding unit estimates of precipitation over the TOGA COARE IFA from Chen et al. (1996) are plotted, as asterisks, against the CRM rainfall rates. Qualitative agreement between the observations and model rainfall rates are good with the observations showing rainfall rates in excess of 1 mm h^{-1} for 20, 21, 22, and 24 December 1992. Chen et al. (1996) show that MCS activity was present over the IFA on those 4 days, and convective cloud systems illustrating the characteristics of MCSs are simulated by the model during the second, third, and fifth days. The horizontal structure of simulated MCSs is shown in Fig. 2: convective columns are shown as dark shading and

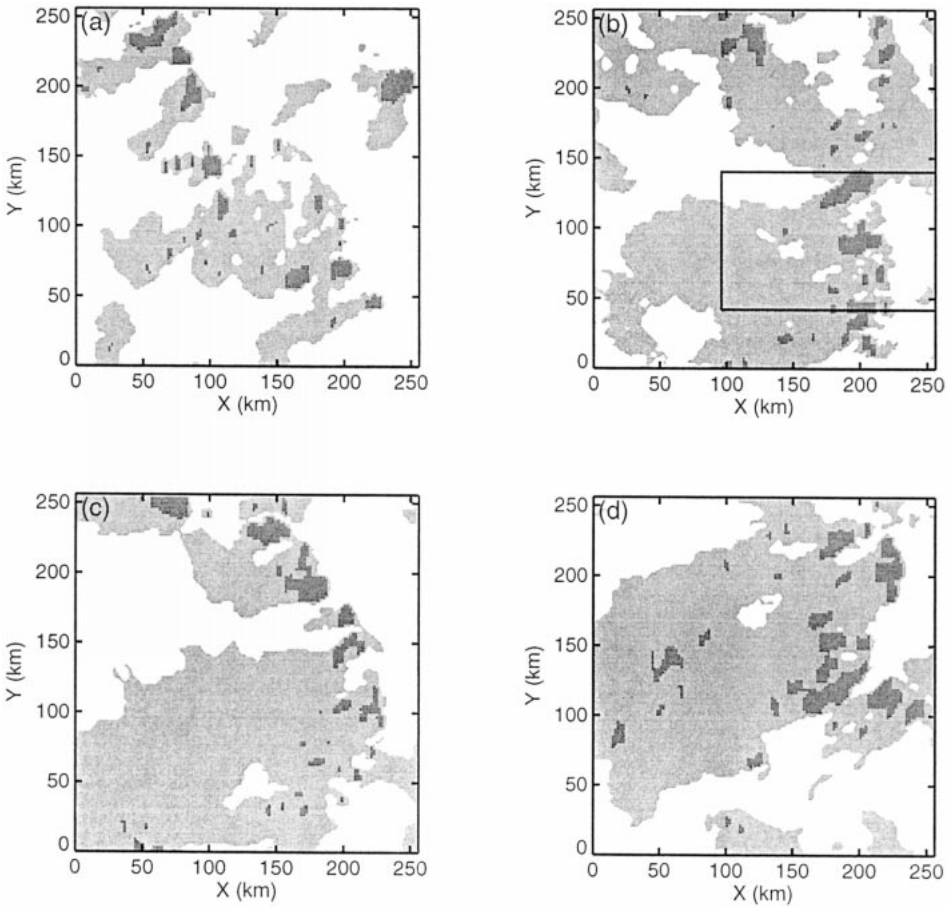

FIG. 2. Horizontal structure of the simulated MCSs at (a) 36 h, (b) 63 h, (c) 69 h, and (d) 111 h. Convective columns are shaded dark gray and stratiform columns light gray. A definition of the column classification used is given in the text. The rectangle in (b) represents the area used in the vertical cross section in Fig. 3.

stratiform columns by light shading. These structures can be compared with the radar observations from TOGA COARE shown by Rickenbach and Rutledge (1998, henceforth referred to as RR). Although it could not be expected that the simulated MCSs show quantitative agreement with radar observations from the IFA for the 20–26 December 1992 period, it is useful to confirm that the structures shown in Fig. 2 are consistent with the examples of TOGA COARE MCSs shown by RR. For example, convective–stratiform partitioning of the radar observations suggests that individual convective regions were generally no bigger than 30 km in size, and usually possessed a longest axis nearer 20 km. This also seems to be the case with the simulated MCSs, although there are slightly fewer convective regions overall, compared to RR's examples, with more at the largest scale. The MCSs simulated on days 3 and 5 (Figs. 2b,c,d) show structures akin to RR's ''MCS linear'' definition, with lines of convective cells at least 100 km in length, with extensive areas of stratiform precipitation. The appearance of small groups of convective cells embedded in the stratiform region in Fig. 2d are also consistent with RR's observations. The day 2 MCS simulated in the model (Fig. 2a) is less organized, and considerably smaller than those modeled on day 3 and day 5. It would likely be classified as ''MCS nonlinear'' by RR, although they classified the MCS they observed in the IFA on 21 December 1992 as linear. The simulated MCSs also show good agreement with conceptual models and observations of MCS in their vertical structure. Figure 3 shows a vertical cross section through the MCS shown in Fig. 2b. Typical features of an MCS, such as the strong convective updrafts, mesoscale updrafts and downdrafts in the trailing stratiform region, plus the development of new cells at a line of convergence where cold pool outflow interacts with the environmental low-level shear, can be seen clearly in the cross section.

Overall, it is fair to say that the model has simulated reasonably realistic MCSs on days 2, 3, and 5. The biggest discrepancy from the observations, however, is that no organized convection was observed on day 1; a cloud cluster was observed over the IFA (Chen et al. 1996). The spinup of the model may be responsible for the failure to successfully simulate that system.

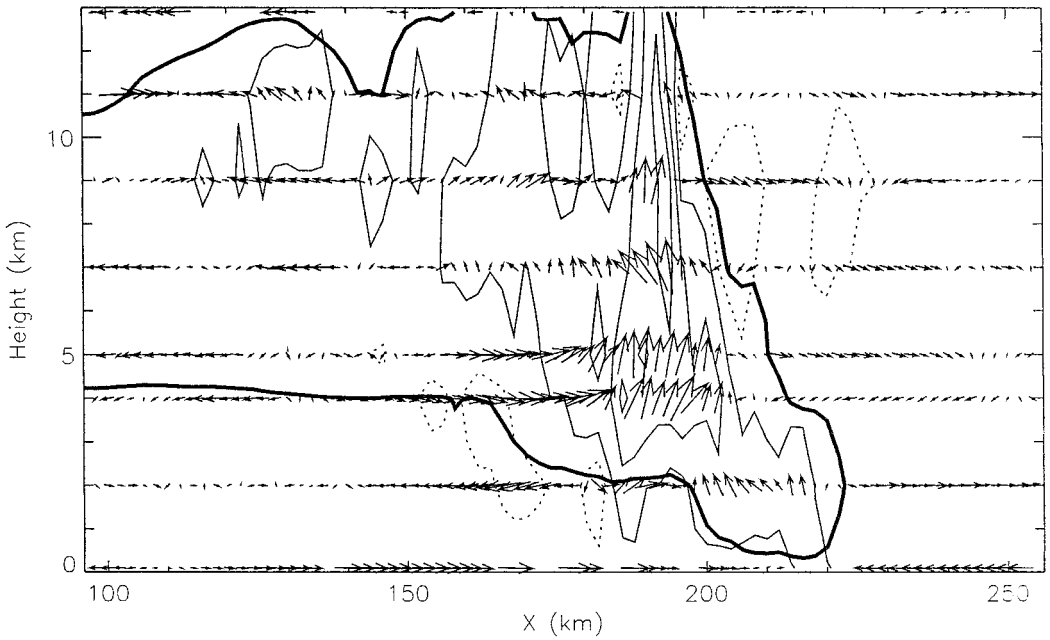

FIG. 3. Vertical cross section of the MCS at 63 h averaged in the *y* direction in the area shown in Fig. 2b. Arrows represent the system relative velocity; the bold contour shows the cloud outline, defined as a mean mixing ratio of 5×10^{-5} kg kg^{-1}; and the thin contours show the mean vertical velocity with contours at ± 0.1, ± 0.5, and ± 1.0 m s^{-1} and negative contours dotted.

The three MCS events described above can provide a dataset for which the properties of tropical MCSs can be determined and used to develop a parameterization. Each model event lasts at least 12 h (Fig. 1), and the properties of each MCS event are determined by averaging over the 9-h period during which the MCS shows its greatest activity and extent. Subsequently, the three events will be referred to as MCS2, MCS3, and MCS5, which correspond to the averaging periods of 30–39 h, 60–69 h, and 108–117 h, respectively, of simulation time.

b. Convective and mesoscale updrafts

Johnson (1984), Houze (1989), and Cheng and Yanai (1989), among others, have demonstrated the importance of the stratiform region in contributing to the total transport in MCSs. This is illustrated in Figs. 4a,b,c, which show the mass fluxes for the convective updraft and mesoscale updraft for MCS2, MCS3, and MCS5, respectively. In all cases the convective updraft mass flux peaks at around the freezing level (4–5 km) and then steadily decreases with height to reach zero at about the 15-km level. The definition of the mesoscale updraft precludes any mass flux below the freezing level, but the mass flux rapidly increases above the freezing level and then remains mostly constant until it falls off after a height of about 11 km. Although just above the freezing level the convective updraft mass flux is roughly 6 times greater than the mesoscale mass flux, toward the top of the MCS the mesoscale updraft is very nearly equal to or, as in MCS3, even slightly greater than the convective updraft mass flux.

The impacts of this on Q_1 and Q_2 are shown for the same three periods in Figs. 4d,e,f. The maximum heating and drying rates associated with the mesoscale updraft is around 5–6 K day^{-1} in MCS3 and MCS5, which compares to maximum convective heating rates in excess of 20 K day^{-1} in MCS5. These are certainly not insignificant and, as with the mass flux, approach the values of convective heating and drying near the top of the MCS.

Figure 4 does indicate that it is worthwhile to attempt to parameterize these mesoscale transports in GCMs, but to be able to do this, first, a better understanding of the properties of the mesoscale updraft needs to be obtained. Properties of the convective and mesoscale updrafts averaged over the three MCS periods are shown in Fig. 5. Figures 5a and 5b show the temperature and water vapor perturbation over the environment, respectively. The convective updrafts are noticeably warmer and moister than the mesoscale updrafts, and the mesoscale updrafts are only barely warmer and moister than the environment. Another key difference is in the hydrometeor content shown in Fig. 5c. Again the hydrometeor content is much greater in the convective updraft. Snow is the dominant hydrometeor in the mesoscale updraft, whereas in the convective updrafts about one-third of the hydrometeor mass is in the form of graupel. Graupel formation requires the presence of liquid water above the freezing level and thus is favored in the strong convective updrafts. It is the higher vertical

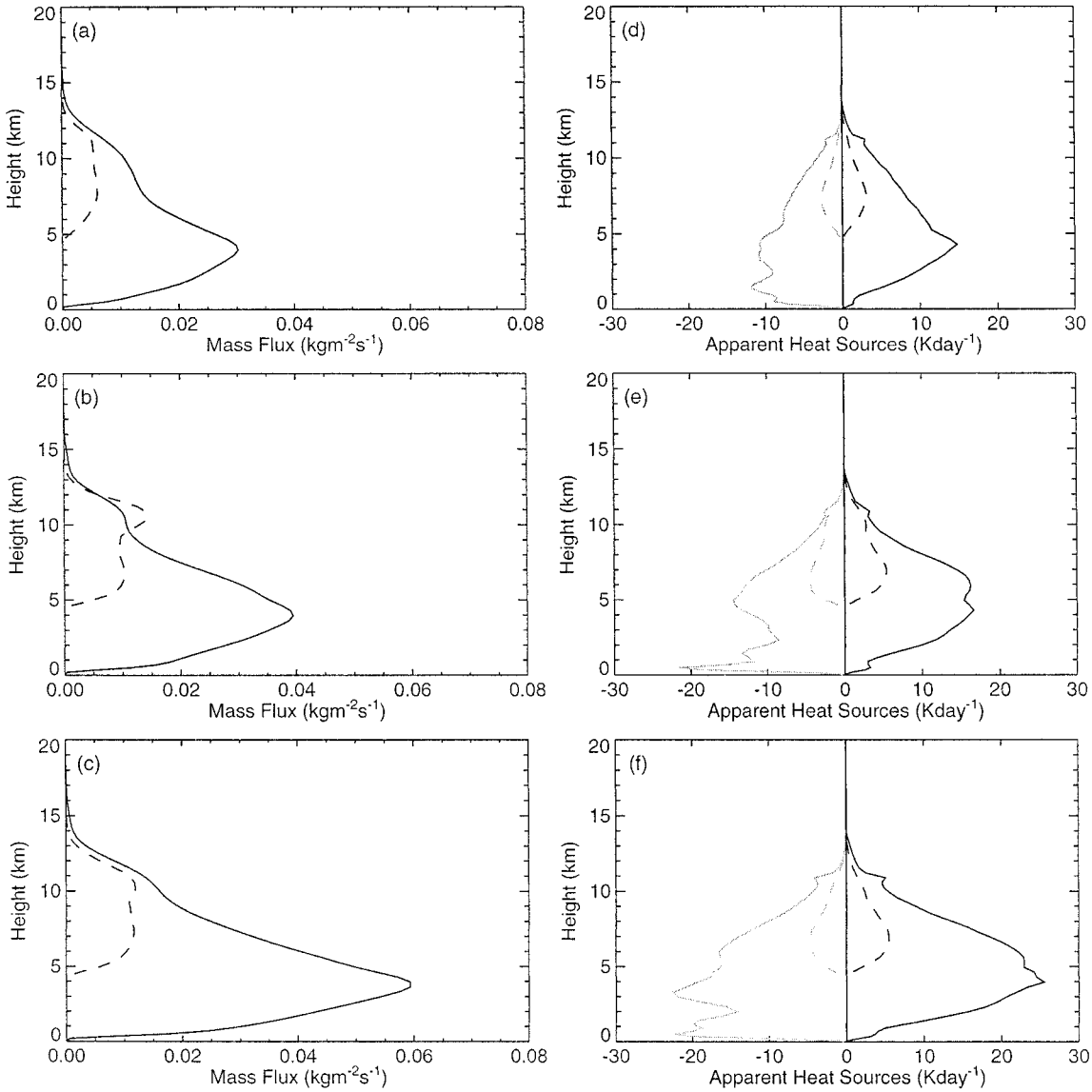

FIG. 4. (a) Nine-hour means of mass flux for MCS2. The solid line represents the convective core mass flux and the dashed line the mesoscale updraft mass flux. (b) as (a) but for MCS3. (c) as (a) but for MCS5. (d) Nine-hour means of Q_1 (black lines) and $-Q_2$ (gray lines) for MCS2. Again the convective updraft is a solid line and the mesoscale updraft the dashed line. (e) as (d) but for MCS3. (f) as (d) but for MCS5.

velocity in the convective updraft, and hence greater vertical transports, which probably account for most of the differences between the convective and mesoscale updrafts. Some graupel is present in the mesoscale updraft, and this may be due to lateral transport of graupel and liquid water from the convective updraft.

Figure 5d compares the virtual temperature perturbation of the convective and mesoscale updrafts, which effectively represents the buoyancy as seen in the model. Although loading due to the hydrometeors has a negative impact on the net buoyancy suggested by the temperature and water vapor perturbations, the convective updrafts are still positively buoyant up to 13 km or so. However, the mesoscale updrafts have little or no buoyancy excess over the environment. This implies that there is little net vertical acceleration in the mesoscale updraft, and so positive vertical velocity can only be maintained if some ascending motion is intially present. It is a widely held view that the stratiform region of an MCS consists of the remnants of old convective cells. The ascent still present in these cells could make an important contribution to the mesoscale updraft in the simulated MCSs. This was suggested by Tao and Simpson (1989), who used back trajectories in their two-dimensional simulation of a tropical squall line to show that the major source of upward mass transport in their

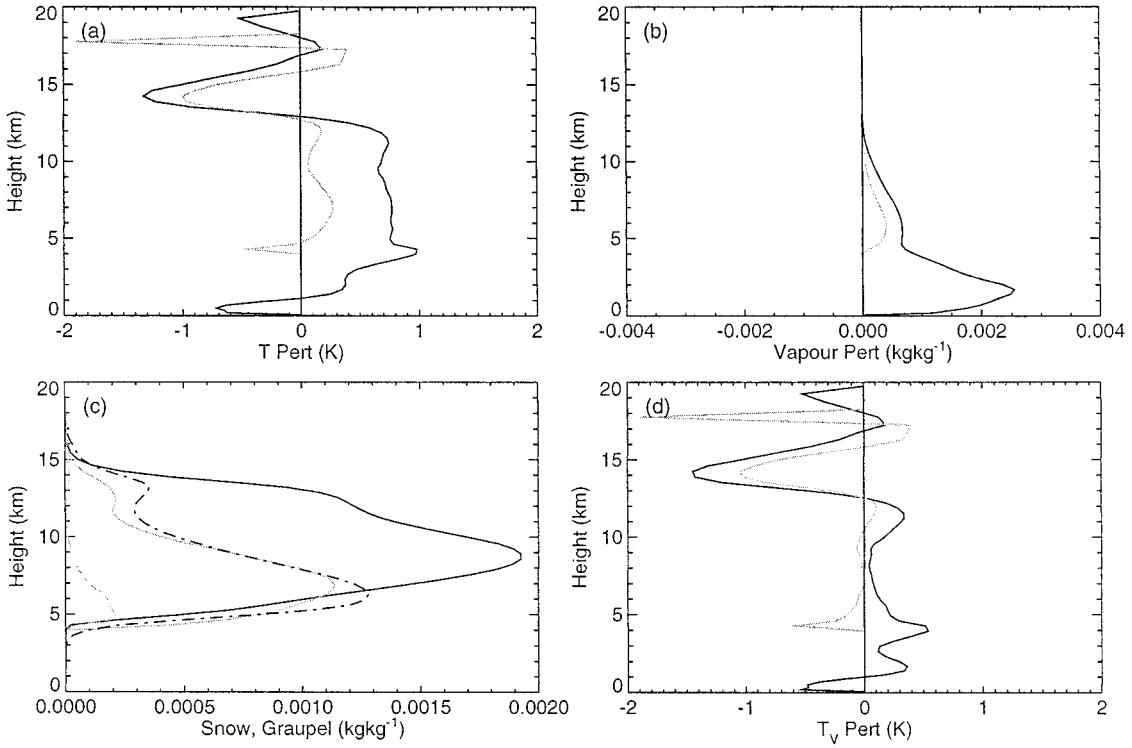

FIG. 5. Mean properties of convective updrafts (black line) and mesoscale updrafts (gray line) for all three MCS periods: (a) temperature perturbation from environment, (b) water vapor perturbation, (c) snow (solid line) and graupel (dash–dot line) mixing ratio, and (d) virtual temperature perturbation from the environment.

anvil region was from older convective updrafts detrained into the anvil region. The mass flux profiles in Fig. 4 certainly show that there is net detrainment from the convective updraft above the freezing level where the mesoscale updraft is present. Hence, the mesoscale updraft could be formed, at least in part, by the detrainment of the convective mass flux.

Horizontal pressure gradients have also been proposed as a possible cause of mesoscale vertical motions in MCSs. Caniaux et al. (1995) showed in their simulations of a tropical squall line that a front-to-rear pressure gradient was established at midlevels. If this pressure gradient were longer than the front-to-rear inflow at this level, then an area of convergence could develop at midlevels, leading to mesoscale ascent and descent. Although the model used by Caniaux et al. (1995) was 2D, similar horizontal pressure gradients are present in the midlevels of the stratiform regions of the MCSs in the 3D simulations here. Areas of convergence are seen, which correspond reasonably well to some of the mesoscale updrafts. Although these horizontal pressure gradients do not extend more than a couple of kilometers up into the anvil, it is probable that these gradients are contributing to the mesoscale updraft at its lowest levels. This is consistent with Fig. 4, which suggests that mesoscale updraft entrainment at its base may be greater than the detrainment from the convective cores. Another possible mechanism that can contribute to mesoscale circulations is radiative destabilization of the anvil through longwave heating at the anvil base and cooling at the anvil top. Such a mechanism was suggested by Donner et al. (1999) for some of their mesoscale circulations. There is some evidence for a radiative effect in these simulations, with mass fluxes for both convective and mesoscale updrafts being higher during periods of net radiative cooling. However, these effects can also be linked to the time variation of the large-scale advective tendencies, and so further study is required before the radiative impact on the mesoscale circulations can be quantified.

c. Precipitating downdrafts

The properties of the precipitating downdrafts, averaged over the three MCS periods and subdivided into those occurring in convective and stratiform columns, are shown in Fig. 6. The mass flux profiles in Fig. 6a suggest that the impact of the mesoscale downdraft is certainly comparable with that of the convective downdrafts in the midtroposphere, although the convective downdraft does seem to dominate toward the top of the mixed layer.

There is a generally good understanding of the processes that lead to the formation of the mesoscale downdraft: snow falling from the anvil changes phase at the melting level, and the cooling this produces, in addition

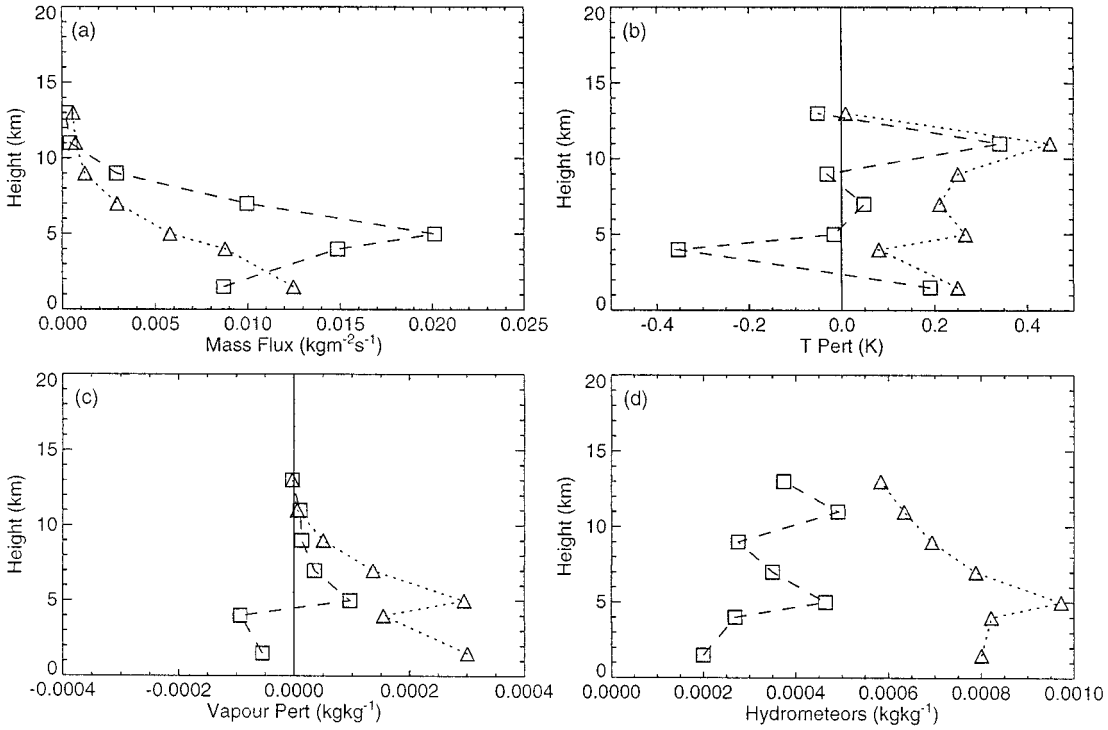

FIG. 6. Mean properties of convective downdrafts (dotted line–triangles) and mesoscale downdrafts (dashed line–squares) for all three MCS periods: (a) mass flux, (b) temperature perturbation from environment, (c) water vapor perturbation, and (d) total hydrometeor content.

to the sublimation and evaporation of precipitation into the dry air beneath, fuels the gentle descent of the downdraft (Houze 1993). Caniaux et al. (1995) have suggested that horizontal pressure gradients may also be important as a source of the mesoscale downdraft. However, Fig. 6b shows the strong cooling present at the melting level indicative of the change of phase, and Fig. 6c illustrates that mesoscale downdraft air is clearly drier than that of the environment below the melting level, suggesting a dominance of the thermodynamic effects. The convective downdraft shows different thermodynamic properties being both warmer and moister than the environment down to the top of the mixed layer. The negative buoyancy of the convective downdraft is thus maintained through the drag of precipitation on the air. This result is consistent with the observational study of Jorgensen and Lemone (1989). The precipitation mixing ratio in the mesoscale downdraft is only a quarter of that of the convective downdraft below the melting level, and hence precipitation drag is less important. The mesoscale downdraft mass flux profile shown in Fig. 6a shows that the mass flux drops off rapidly below the melting level. This suggests that the mesoscale downdraft is driven by the sublimation, evaporation, and phase change at the melting level, but beneath that level evaporation does not necessarily counter the adiabatic warming of descent. The decrease in mass flux represents erosion of the mesoscale downdraft due to loss of negative buoyancy or complete evaporation of precipitation. The convective downdraft mass flux increases beneath the melting level. This is likely to be due to the entrainment of environmental air into the downdraft and an augmentation to the downdraft through precipitation falling out of the tilted convective updraft.

Cold pools are observed at the surface, however, which suggests that the downdrafts do not remain warm for their full descent. As the downdrafts approach the surface, they are seen to cool substantially. For example, in MCS5 the mean downdraft temperature is 1.5 K greater than the environment at 1.5 km but 0.6 K lower than the environment at 500 m. This change can be attributed to reductions in stability (0.005 K m^{-1} at 3 km; 0.003 K m^{-1} at 1 km) and increases in the saturation deficit (0.001 kg kg^{-1} at 3 km; 0.002 kg kg^{-1} at 1 km) toward the surface. This leads to reductions in the adiabatic warming and increases in rainwater evaporation respectively, thus leading to a cooling of the downdraft.

d. Momentum transports

The importance of vertical transports of horizontal momentum in the atmospheric general circulation have been emphasized in many studies (e.g., Houze 1973), and successful parameterizations for this process have been developed (e.g., Gregory et al. 1997). The mesoscale updraft and downdraft have been shown to have some impact on the heat and moisture fields, so it is

reasonable to ask whether they have any effect on the horizontal momentum fields.

Time–height plots of zonal (x direction) momentum flux for the entire CRM simulation are shown in Fig. 7. Comparison of the total momentum flux (Fig. 7a) and the convective updraft momentum flux (Fig. 7b) shows that the latter dominates through most of the troposphere. The sign reversal in the vertical in the convective updraft momentum flux can be attributed to variations in the mean wind profile with height. This is illustrated in Fig. 8, where the mean convective updraft zonal velocity is plotted against the domain mean zonal velocity during MCS5. The shear within the convective updraft is somewhat less than the domain mean, as anticipated by the parameterization theory of Gregory et al. (1997), for example, which leads to a negative velocity perturbation in the updraft below a height of 5 km and a positive velocity perturbation between 5 and 7 km. This is consistent with the change in sign of momentum flux at these levels seen in Figs. 7a and 7b. Although the convective updraft momentum flux dominates, Fig. 7c does show that during the intense convection periods of MCS3 and MCS5 the precipitating downdrafts provide some significant momentum transports in the lower troposphere. The mesoscale updraft (Fig. 7d), on the other hand, is associated with very little momentum transport. Although the values are nonzero, they are nearly negligible compared to the transports in the convective updrafts. A similar result was obtained for the CRM experiments of Cotton et al. (1996), and it is reasonable to assume that the mesoscale updraft can be neglected for the parameterization of momentum transports. Cotton et al. (1996) suggested that momentum transport in the gravity waves generated by the MCS were of more importance, and this can be seen in the simulations here by comparing Figs. 7a and 7b; there is significant momentum flux at higher model altitudes that cannot be attributed to the convective-scale updrafts.

Although the mesoscale updraft does not contribute significantly to the total momentum transport, there is evidence that the mesoscale downdraft may have momentum transports akin to those in the convective downdraft. For example, at the 1.5-km level during MCS5 the zonal momentum transport in the precipitating downdrafts in convective columns is -0.0252 m^2 s^{-2} whereas it is -0.0198 m^2 s^{-2} in the stratiform columns. Furthermore, Fig. 8 shows that the precipitating downdrafts have a markedly accelerated zonal wind component in the lowest 4–5 km compared to the domain mean wind. This is noted in both the convective ($+1.16$ m s^{-1}) and mesoscale ($+1.04$ m s^{-1}) components at 1.5 km. Simple downgradient transport of momentum would imply that the downdraft zonal velocity would be less than that of the environment, and hence the momentum fluxes would be positive. The downdraft horizontal velocities must be being accelerated by some other mechanism to explain this. MCSs have been observed to have rear-to-front inflow beneath the stratiform anvil, possibly associated with horizontal pressure gradients. With the orientation of the MCSs shown in Fig. 2 the rear inflow would be expected to be in primarily a zonal direction. Both convective and mesoscale downdrafts will have their zonal wind affected by this rear-to-front inflow, and as the two downdraft components have similar mass fluxes (cf. Fig. 6a) their zonal momentum fluxes will be comparable.

The mesoscale organization of the MCS does not impact on the meridional momentum fluxes in the same way. The convective downdraft meridional momentum fluxes is -0.013 m^2 s^{-2} at 1.5 km during MCS5 whereas it is $+0.003$ m^2 s^{-2} in the mesoscale downdraft. This is consistent with a meridional wind perturbations of $+0.29$ m s^{-1} and -0.33 m s^{-1} in the convective and mesoscale downdrafts, respectively. These fluxes can be understood in terms of downgradient transport. The mesoscale downdraft can be thought of being primarily formed at the freezing level, and here the meridional wind is at a minimum. This would tend to give a negative wind perturbation and hence a positive momentum flux. The convective downdraft seems to entrain air over a greater depth and hence would not necessarily possess a meridional velocity less than that of the environment.

The effects of the mesoscale organization in MCSs are generally not considered in operational convective momentum transport schemes, such as Gregory et al. (1997). However, it is suggested here that organization in MCSs can change the sign of the downdraft momentum transport when compared to simple downgradient theory. This supports the results of the dynamical models of Moncrieff (1992), in that horizontal mesoscale circulations, such as the rear inflow, can play an important part in determining the total momentum transport of organized convective systems.

4. Parameterization for mesoscale scalar transports

The parameterization approach for the mesoscale transports presented here differs somewhat from other studies such as Cheng and Yanai (1989), Donner (1993), and Alexander and Cotton (1998). From Cheng and Yanai (1989) the apparent heat source and moisture sink due to the mesoscale transports (Q_{1m} and Q_{2m}, respectively) can be written as (their 2.14 and 2.15)

$$Q_{1m} = L(c_m - e_m) - \frac{\partial}{\partial z}[(M_m - \sigma_m \overline{M})(s_m - \tilde{s})] \quad (3)$$

$$Q_{2m} = L(c_m - e_m) + L\frac{\partial}{\partial z}[(M_m - \sigma_m \overline{M})(q_m - \tilde{q})], \quad (4)$$

where m subscripts refer to properties of the mesoscale components; overbars to large-scale means and tildes to environmental properties; with M representing the mass flux; s the dry static energy; q the specific humidity; c and e condensation and evaporation, respectively; and σ the fractional area. It has been assumed for convec-

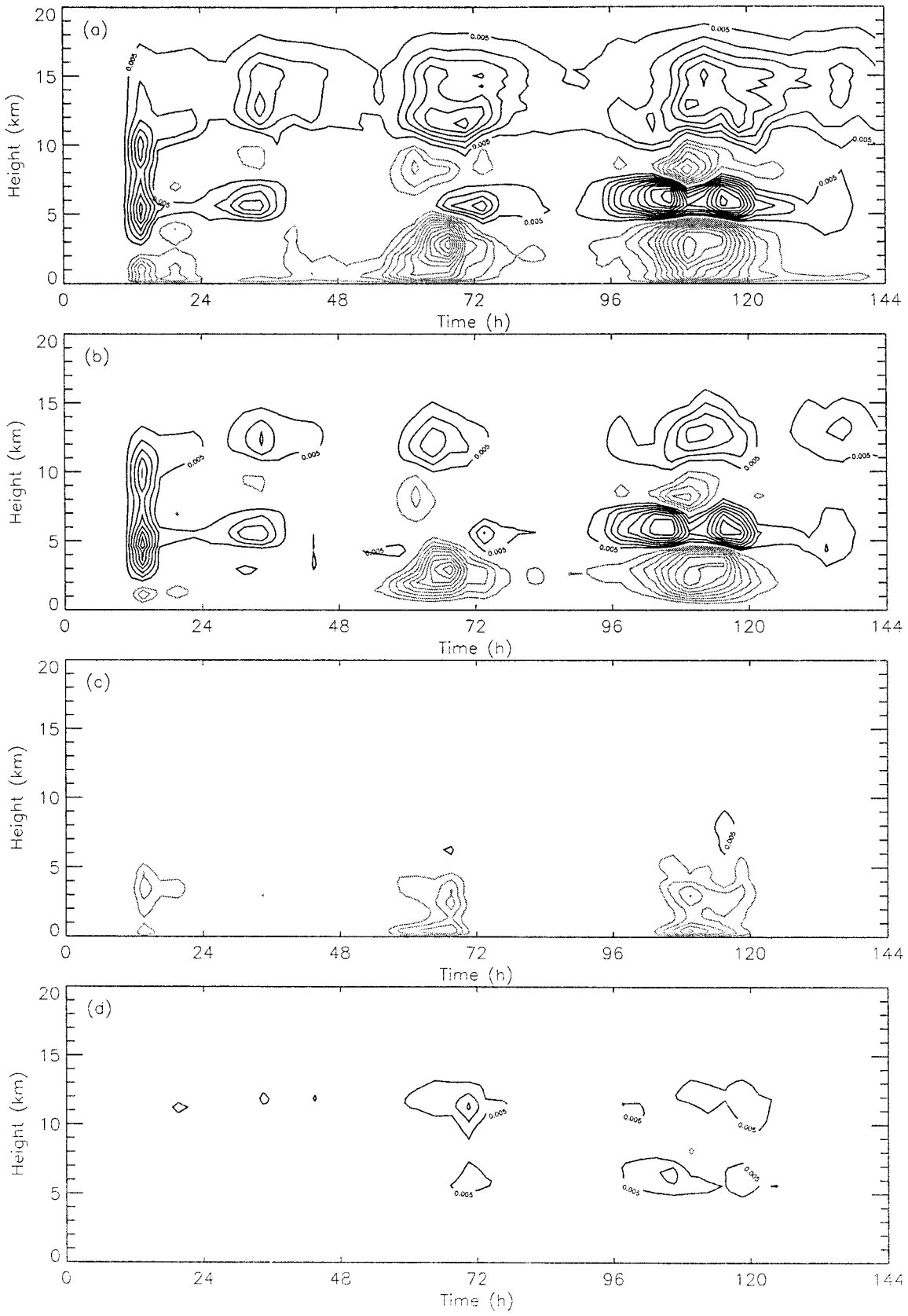

FIG. 7. Zonal momentum flux diagnosed from the CRM simulation for (a) all points, (b) convective updrafts, (c) precipitating downdrafts, and (d) mesoscale updrafts. Contour interval is 0.01 m^{-2} s^{-2}, first contour at 0.005 m^{-2} s^{-2}, and negative values are shown in gray.

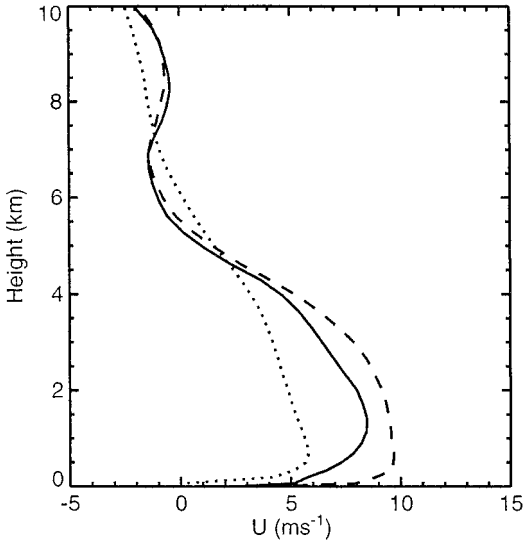

FIG. 8. Mean zonal wind speed for MCS5 for the whole domain (solid line), convective updrafts (dotted line), and the precipitating downdrafts (dashed line).

tive-scale updrafts and downdrafts (Yanai et al. 1973) that $\sigma \ll 1$. Even when assuming a generous averaging scale such as the 250 km represented by the CRM domain, this assumption is unlikely to be valid for mesoscale updrafts; in the CRM experiments the mesoscale updrafts occupied up to 20% of the domain area. Cheng and Yanai (1989) suggest that the eddy flux terms in (3) and (4) can be neglected as

$$M_m - \sigma_m \overline{M} = M_m\left(1 - \frac{\overline{\omega}}{\omega_m}\right) \tag{5}$$

and the ratio of the environmental vertical velocity ($\overline{\omega}$) to the mesoscale vertical velocity (ω_m) may be of the order unity. Comparisons of the vertical velocity implied by the large-scale forcings and that typified for the mesoscale updraft (25 cm s^{-1}) from the CRM experiment suggest that this may not be the case. However, the CRM simulations indicate that $s_m \approx \overline{s}$ (Fig. 5a). This, similarly, allows the eddy flux term in (3) to be neglected, and hence

$$Q_{1m} \approx L(c_m - e_m). \tag{6}$$

It is possible to determine an expression for c_m for the mesoscale updraft using the continuity equation for s (after Yanai et al. 1973). This can be written as

$$E\overline{s} - Ds_m - \frac{\partial}{\partial z}M_m s_m + Lc_m = 0, \tag{7}$$

where E and D are the rates of entrainment and detrainment for the plume, respectively, given in the equation

$$\frac{\partial M_m}{\partial z} = E - D. \tag{8}$$

Rearranging (7) and substituting in (8) gives

$$Lc_m = M_m\frac{\partial s_m}{\partial z} + E(s_m - \overline{s}). \tag{9}$$

Again, using the assumption that $s_m \approx \overline{s}$, (9) can be expressed as

$$Lc_m = M_m\frac{\partial \overline{s}}{\partial z} \tag{10}$$

and, hence, (6) as

$$Q_{1m} = M_m\frac{\partial \overline{s}}{\partial z} - Le_m. \tag{11}$$

The evaporation term can be incorporated by assuming that some fraction, γ, of the condensate may detrain from the plume and evaporate into the environment. Thus, (11) becomes

$$Q_{1m} = (1 - \gamma)M_m\frac{\partial \overline{s}}{\partial z}, \tag{12}$$

where the disposable parameter, γ, can be prescribed or, alternatively, calculated from the mass detrainment rates to give the fraction of condensate detrained.

Equation (12) gives the condensation–evaporation term which, for consistency, can be substituted into (4). However, for humidity it is not reasonable to neglect the eddy flux term. Typically, the environmental relative humidity is about 80% in the CRM during the MCS periods, whereas the mesoscale updraft must be saturated by definition. Therefore, to calculate the eddy flux term it is assumed that q_m can be approximated to the local saturation value over ice, q_s. Hence, (4) becomes

$$Q_{2m} = Q_{1m} + \eta L\frac{\partial}{\partial z}[M_m(q_s - \tilde{q})], \tag{13}$$

where η is a disposable parameter representing $(1 - \overline{\omega}/\omega_m)$.

The validity of this parameterization approach can be evaluated, and values for the disposable parameters determined, by comparing the parameterization expressions (12) and (13) to the full Q_{1m} and Q_{2m} terms given in (3) and (4) for the mesoscale updraft conditionally sampled diagnostic in the CRM experiment. Such comparisons can be seen for the first 3 h of MCS3 and MCS5 in Figs. 9a and 9b, respectively. Using a value of γ of 0.2 in the calculation of the parameterized Q_{1m} (solid gray line) gives fairly good agreement with the calculated Q_{1m} shown by the solid black line. However, there is a suggestion that γ is not universal with height, and determining the fraction from the model detrainment rates may prove to be a better approach in the parameterization. The eddy flux term for Q_{1m} is negligible as witnessed by the dotted line. Good agreement for the calculated and parameterized Q_{2m} is also seen (black and gray short-dashed lines), but now the eddy flux term is not as insignificant as for Q_{1m} (black dash–dot line). However, the suggested parameterization (gray dash–dot line) using $q_m \approx q_s$ and $\eta = 1$ gives very good

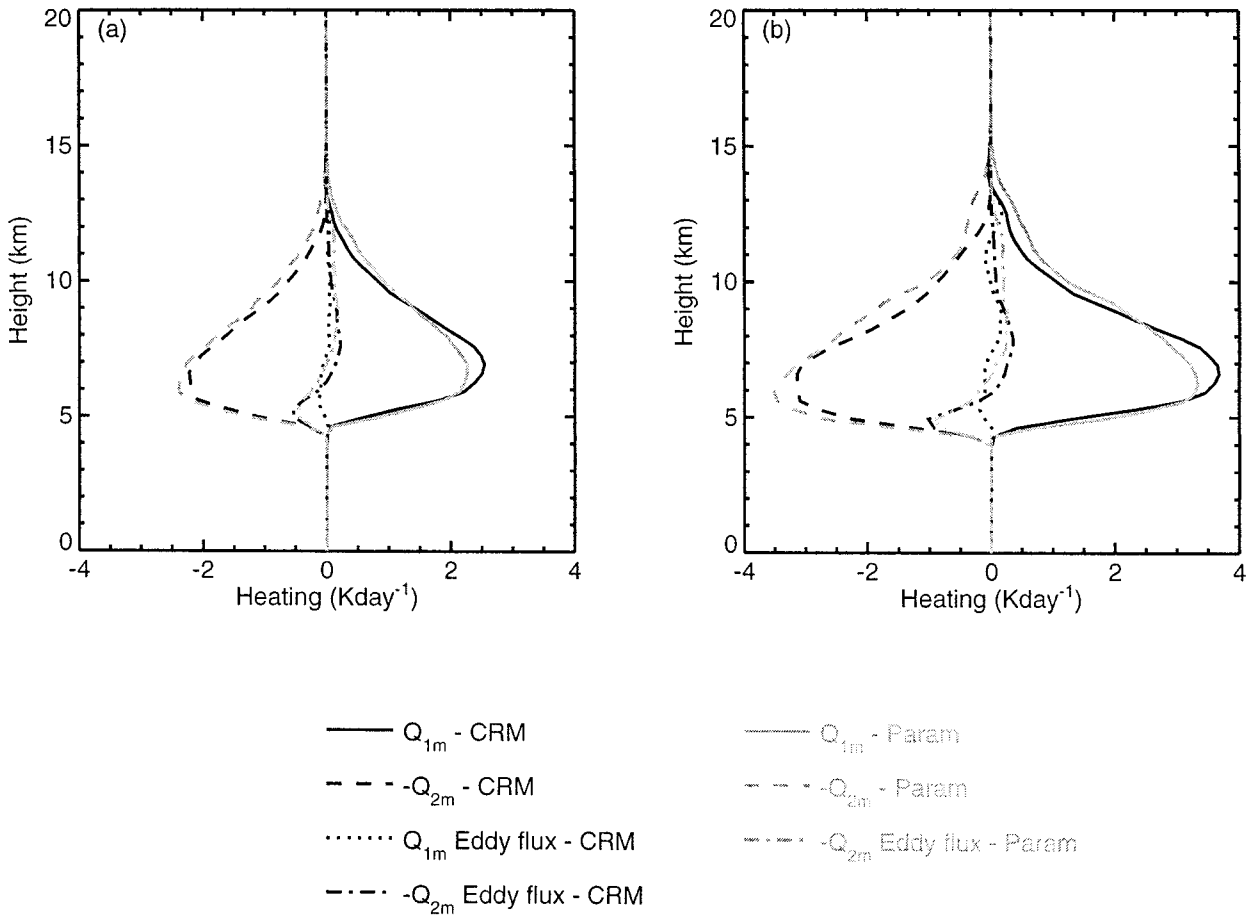

FIG. 9. Comparisons of the diagnosed Q_{1m} and Q_{2m} from the CRM experiment as given by (3) and (4) and the parameterized Q_{1m} and Q_{2m} as suggested by (12) and (13) for (a) the first 3 h of MCS3 and (b) the first 3 h of MCS5.

agreement. These comparisons suggest that the parameterization approach proposed above is valid for the mesoscale updrafts for the simulated MCSs.

These parameterizations for the mesoscale updraft require knowledge of the mesoscale updraft mass flux. In section 3b it was argued that the mesoscale updraft could be thought of as being formed by the detrained convective mass flux. This notion will be used to close the mass flux equation given in (8) by defining the entrainment rate as

$$E = \varepsilon_m M_m + \alpha \delta_c M_c, \tag{14}$$

where ε_m is the fractional mass entrainment coefficient for the mesoscale updraft, δ_c is the fractional mass detrainment coefficient for the convective updraft, M_c is the convective updraft mass flux, and α represents the fraction of detrained convective mass flux that enters the mesoscale updraft. It should be noted that for the derivation of (10) to follow from (7) with this definition of E, it must be assumed that the dry static energy of the detrained convective air is close to that of the environment. Both M_m and α are taken to be zero at all levels below the freezing level.

A simple microphysics-based scheme is used to represent the mesoscale downdraft. Rutledge and Houze (1987) found that lateral transport of snow from the convective cells into the stratiform region contributed significantly to the development of stratiform precipitation. This is modeled by assuming that some of the precipitation from the convective cores is detrained into the anvil region. This precipitation grows through accretion of the condensate generated by the mesoscale updraft and that present in the large-scale cloud field. At and below the freezing level, melting and evaporation of precipitation occurs that acts to cool and moisten the environment. The accretion and evaporation rates are determined from the CRM simulation.

This simple parameterization does, however, neglect the eddy flux terms. Other studies show that the eddy fluxes in the mesoscale downdraft may not be large when compared to the effects of precipitation phase changes (e.g., Xu 1995). In addition, there is some uncertainty over the convective downdraft parameterization. The CRM results presented in Fig. 6 suggest that the convective downdraft is warm and moist, whereas the parameterization models a cold saturated plume. In-

cluding some representation of the mesoscale downdraft eddy fluxes may, therefore, be considered an unnecessary over complication when considering the total downdraft response.

5. Single-column model tests

The same dataset of temperature and specific humidity tendencies that was used to force the CRM is used to force the single-column version of The Met. Office Unified Model (SCM). The SCM is configured with 30 vertical levels and run with a half-hour time step. The convection parameterization is a modified version of the Gregory and Rowntree (1990) bulk mass flux scheme using a convective available potential energy closure and including a representation for downdrafts and convective momentum transports (Gregory et al. 1997). The formulation of detrainment from the convective plume is different from that of the original Gregory and Rowntree scheme; detrainment is set greater than entrainment above the level of minimum equivalent saturated potential temperature, which gives better agreement with CRM mass flux profiles. The boundary layer turbulence parameterization is that described by Smith (1990) in which mixing coefficients depend on a local Richardson number and a mixing length. A large-scale cloud parameterization is included that calculates cloud amount and water content by assuming a simple distribution of thermodynamic and water content variables about their grid-box mean values, also described by Smith (1990). Due to uncertainties in the interaction between the convection and radiation parameterization schemes, the radiation scheme is replaced by the mean net radiative forcing diagnosed from the CRM. This ensures that the total thermodynamic forcing is comparable between the CRM and SCM runs.

The mesoscale updraft and downdraft parameterizations are coded as described in the previous section. The disposable parameters are set as follows: γ is calculated from the mesoscale detrainment rate; η is equal to 1, following the CRM comparison (Fig. 9b); and α is taken as 0.75. The exact value of α selected is a purely pragmatic choice for this case, but observations of MCS budgets by Leary and Houze (1980) suggest that convective air is detrained into the environment and the stratiform region in the ratio of roughly 1 to 4, so the value selected is quite reasonable. The mesoscale entrainment and detrainment rates, ε_m and δ_m, are defined as functions of the convective entrainment and detrainment rates, ε_c and δ_c, such that in the 200 mb immediately above the freezing level $\delta_m = \delta_c$ and $\varepsilon_m = 2 \times \varepsilon_c$ and elsewhere $\delta_m = 2 \times \delta_c$ and $\varepsilon_m = \varepsilon_c$. These values are chosen as they effectively represent the shallow depth of net entrainment at the base of the mesoscale updraft and the deeper layer of net detrainment at the top. Again there is some pragmatism in the choices of ε_m and δ_m, although the increased entrainment around the freezing level could reasonably be argued to be representing any increase in the mesoscale updraft through the dynamical effects of horizontal pressure gradients.

An outstanding issue is when to switch on the mesoscale anvil parameterization. This requires some diagnosis of the organization of convection. Many studies (e.g., Thorpe et al. 1982) have shown the importance of low-level shear in the organization of convection, so for the purposes of the experiment here, convection is considered to be organized into an MCS-like structure if the convective cloud top is higher than 300 mb and low-level shear is greater than 0.002 s^{-1}. This provides a reasonable diagnosis for this TOGA COARE simulation.

Figure 10 shows contour plots of the convective and mesoscale updraft heating rates for both the CRM and SCM experiments. The parameterized mesoscale updraft heating rate (Fig. 10d) from the SCM run agrees fairly well with that diagnosed from the CRM experiment (Fig. 10c) in magnitude, depth, and timing. This appears to be best on day 5 when the convective heating rates also agree well between the two experiments. The convective heating seems to be fairly uniform in the SCM on the first 3 days when compared to the CRM experiment, and one result of this may be the weaker mesoscale updraft heatings observed. As the mesoscale updraft parameterization is driven by the convective parameterization through the detrainment of mass, any shortfall in the convective parameterization will be reflected in the mesoscale updraft parameterization. This is an inevitable problem of such a linking, the solution to which is to improve the original convective parameterization scheme. The purpose of these experiments, however, is to evaluate the mesoscale transport parameterization described in the previous section, and this can be achieved by comparing the models on day 5 when their respective convective heating rates are similar.

The mean mass fluxes for day 5 for the convective and mesoscale updrafts are plotted in Fig. 11a. In this case, good agreement in the convective mass fluxes leads to excellent agreement in the mesoscale mass fluxes. (The apparent large discrepancies in the convective mass fluxes near the surface can be accounted for by the absence of shallow convection in the conditionally sampled convective updraft diagnostic.) It is not too surprising, with such good agreement in the mass flux profiles, that the convective and mesoscale updraft heating rates also agree well. A similar result is obtained for the moistening due to the mesoscale updraft as seen in Fig. 11c.

The SCM convective and mesoscale downdraft heating and moistening terms have been combined for comparison with the CRM in Figs. 11b and 11c. This is because no reliable conditional diagnostic to distinguish between the two was used in the CRM. Both the heating and moistening terms agree reasonably well with those diagnosed from the CRM. The melting level peak due to phase change seems too big in the SCM compared to the CRM. In the CRM, rapidly falling hydrometeors,

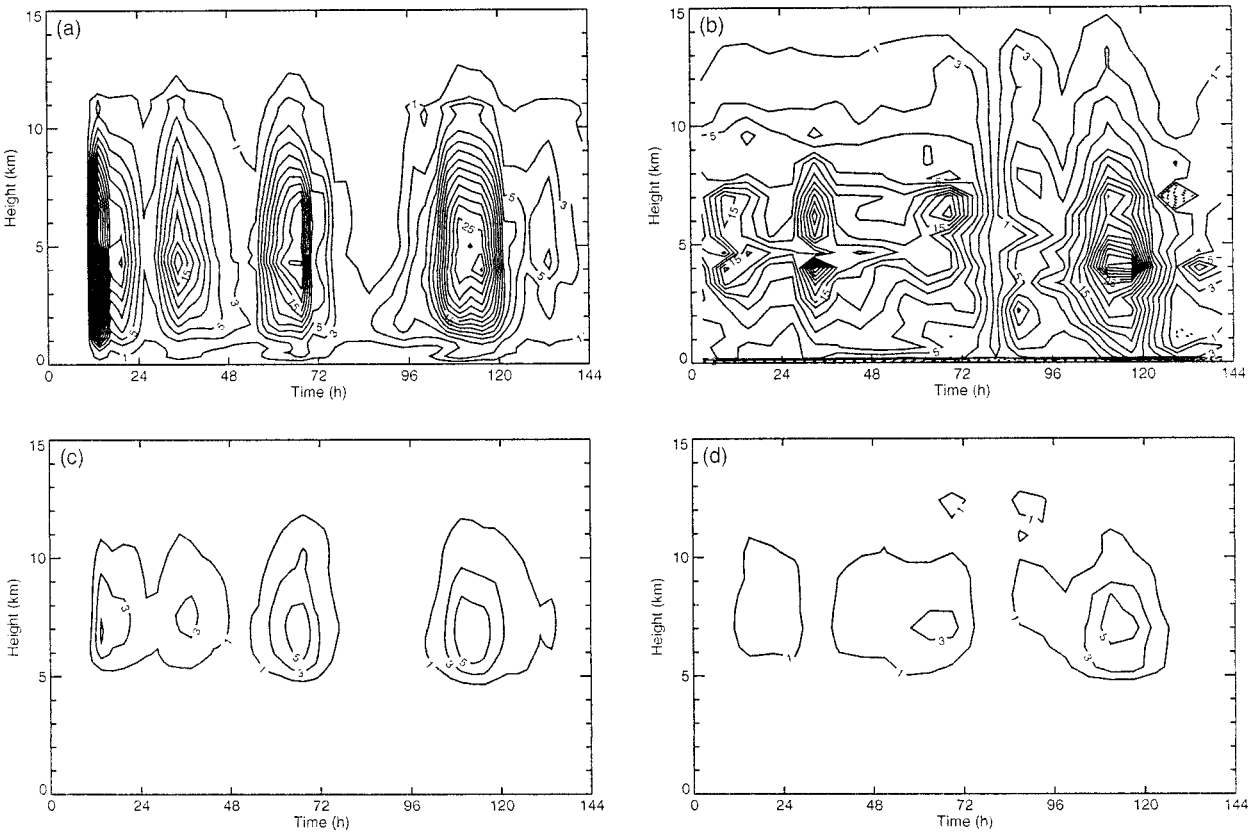

FIG. 10. Convective updraft heating rates for (a) CRM and (b) SCM experiments, and (c) mesoscale updraft heating rates for CRM and (d) SCM. Contour interval is 2 K day^{-1} with the first contour at 1 K day^{-1}.

such as graupel, melt in a layer a couple of kilometers beneath the melting level; the convective parameterization melts all hydrometeors at the melting level. Also, the parameterization seems to underestimate evaporation of precipitation above the freezing level. The surface precipitation rate is a bit higher in the SCM at 1.62 mm h^{-1} compared to 1.24 mm h^{-1} for the CRM on day 5. The proportion of rainfall that is stratiform is 28% in the SCM as opposed to 20% in the CRM. The convection parameterization scheme seems to overestimate the precipitation rate which feeds through into the mesoscale rain rate. This is another example of where accuracy in the convection scheme is essential for the mesoscale parameterization to perform well.

However, the mesoscale parameterization does improve the representation of the convective heating and moistening rates compared to an SCM experiment in which the parameterization is not included. Figure 12 shows a comparison of the total convective Q_1 and Q_2 for the CRM experiment, the SCM experiment including the mesoscale transport parameterization (SCM-Mes), and an identical SCM experiment except without the parameterization (SCM-Cntl). SCM-Mes shows a much better agreement with the CRM heating and moistening profiles than SCM-Cntl does. This improvement can be attributed to the heating and moistening dipole due to the mesoscale circulations, which is absent in SCM-Cntl. This is most marked in the heating profile in Fig. 12a, where the SCM-Cntl profile shows too much heating below 5 km and too little heating above. The additional heating provided by the mesoscale updraft above 5 km and the extra cooling due to the mesoscale downdraft below 5 km shifts the heating profile in SCM-Mes much closer to that measured in the CRM. It appears that the mesoscale parameterization presented here has performed very successfully in the SCM simulation. The comparison between SCM-Mes and SCM-Cntl gives encouragement that the scheme will improve the representation of heating and moistening of MCSs in lower resolution GCMs, where the mesoscale circulations are not resolved.

It must be noted that the parameterization has only been evaluated against this single, albeit extensive, TOGA COARE case. Characteristics of MCSs may vary depending on the environmental conditions, and consequently the choices of disposable parameters used here may not prove to be the optimal values if the scheme were included in a GCM.

6. Summary

A cloud-resolving model has been used to study the properties of simulated MCSs and to propose a param-

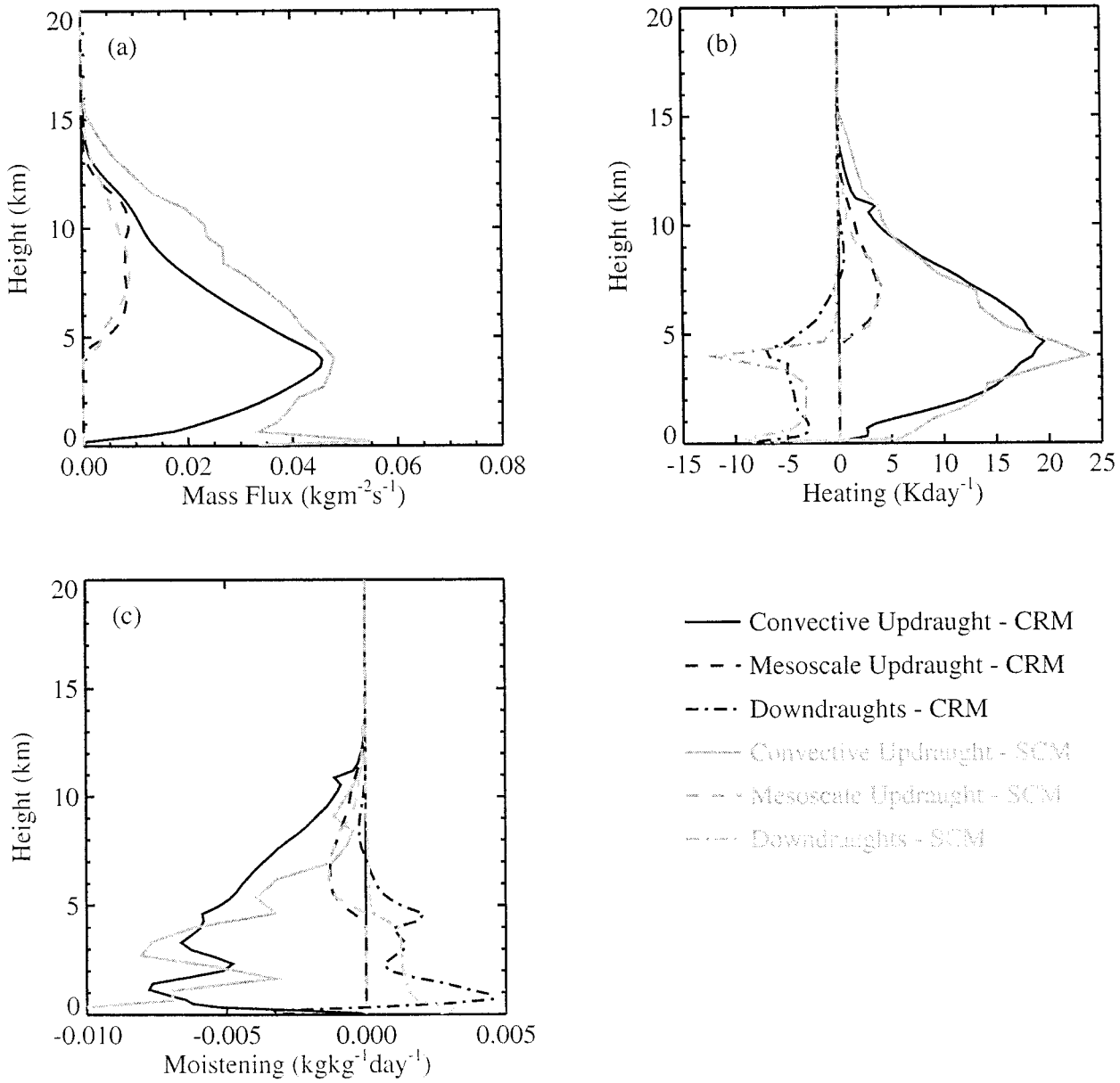

FIG. 11. Comparison of (a) mass fluxes, (b) heating rates, and (c) moistening rates between the CRM and SCM simulations averaged over day 5 of the simulation. Convective updrafts are shown by solid lines, mesoscale updrafts by dashed lines, and downdrafts by dash–dot lines. Results from the CRM are shown as black lines and results from the SCM are shown as gray lines.

eterization for the mesoscale scalar transports. Using forcing data from a westerly wind burst event in December 1992 from TOGA COARE, simulations of three MCSs have been performed. Conditional sampling diagnostics have attempted to subdivide the model domain into convective updrafts, mesoscale updrafts, and precipitating downdrafts in order to study the properties of these components of the MCS circulation. As with other studies, the CRM experiment has shown that the mesoscale updraft is associated with heating and drying rates of up to 6 K day^{-1} in the upper troposphere, which are comparable with those diagnosed for the convective updrafts in the same region. Convective momentum transport is dominated by the convective updrafts, and although not zero, the momentum transports associated with the mesoscale updraft are small enough to be neglected in comparison. On the other hand, the momentum transports due to the downdrafts are significant during the periods of organized convection, of similar magnitude in both the convective and mesoscale downdraft, and apparently countergradient. It appears that a rear-to-front inflow associated with the MCS circulations

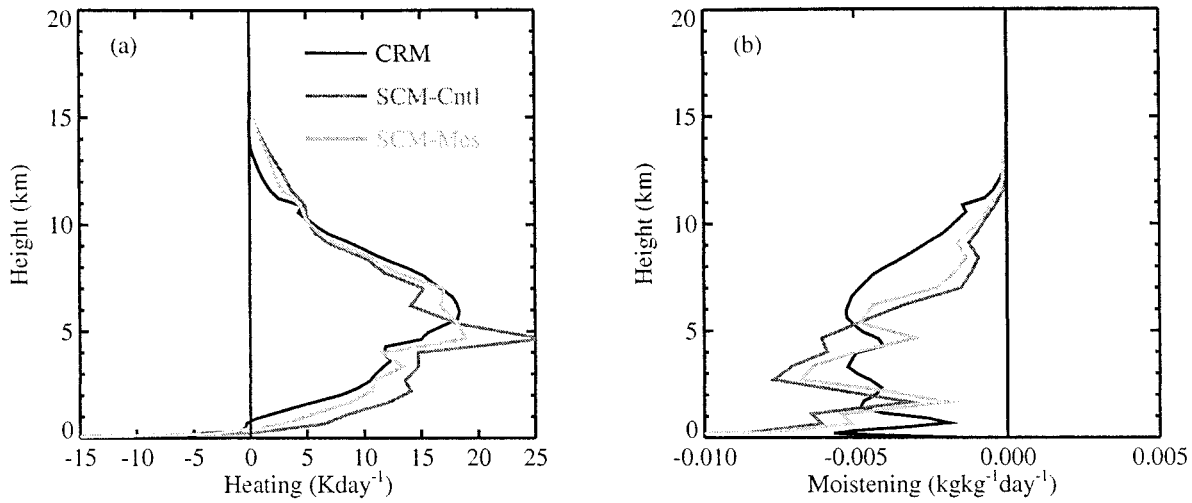

FIG. 12. Comparison of (a) apparent convective heat source and (b) apparent convective moisture source, averaged over day 5 for the CRM (black line), the SCM without a mesoscale updraft and downdraft parameterization (SCM-Cntl, medium gray line), and the SCM with a mesoscale updraft and downdraft parameterization (SCM-Mes, light gray line).

could be accelerating the downdraft circulations with respect to the environment leading to these stronger momentum fluxes.

The mesoscale updraft seems to be barely buoyant in the CRM simulation, which may imply that some other factor is responsible for the upward motion. In keeping with conceptual models of MCSs, it is suggested that decaying convective cells are, in part, responsible for the mesoscale ascent. This notion is used in a mass flux parameterization for the mesoscale updrafts. The mesoscale updraft is assumed to have the same dry static energy as the environment, to be at saturation, and to be formed by the entrainment of a fraction of the detrained mass flux from the convective updraft above the freezing level. This parameterization, along with a simple representation of the mesoscale downdraft, is included in a single-column model that is run for the same TOGA COARE period as the CRM. On day 5 of the simulation, when the single-column and CRM convective updraft mass fluxes concur, excellent agreement is shown between the CRM results and the heating and moistening rates determined by the mesoscale scalar transport parameterization. The agreement is poorer when the mesoscale parameterization is removed. This gives confidence that such a parameterization scheme could be of benefit to GCMs.

Some uncertainties remain, in particular, the diagnosis of when to use the mesoscale transport parameterization, representation of the mesoscale downdraft eddy fluxes, and changes to the parameterization of convective momentum transports to account for the MCS organization. However, these are of secondary importance to the need for an accurate parameterization of the deep convective-scale circulations that drive the mesoscale parameterization.

Acknowledgments. Thanks to Jon Petch for interfacing the radiation scheme with the CRM, to Steven Krueger for his coordination of the GCSS Working Group 4 Case 2 through which the TOGA COARE dataset was available, and to Julie Gregory for assistance in running the single-column model. Thanks also to Dave Gregory and two other reviewers for useful comments on earlier versions of this manuscript.

REFERENCES

Alexander, G. D., and W. R. Cotton, 1998: The use of cloud-resolving simulations of mesoscale convective systems to build a mesoscale parameterization scheme. *J. Atmos. Sci.,* **55,** 2137–2161.

Brown, A. R., S. H. Derbyshire, and P. J. Mason, 1994: Large-eddy simulation of stable atmospheric boundary layers with a revised stochastic subgrid model. *Quart. J. Roy. Meteor. Soc.,* **120,** 1485–1512.

Caniaux, G., J.-P. Lafore, and J.-L. Redelsperger, 1995: A numerical study of the stratiform region of a fast-moving squall line. Part II: Relationship between mass, pressure, and momentum fields. *J. Atmos. Sci.,* **52,** 331–352.

Chen, S. S., R. A. Houze, and B. E. Mapes, 1996: Multiscale variability of deep convection in relation to large-scale circulation in TOGA COARE. *J. Atmos. Sci.,* **53,** 1380–1409.

Cheng, M.-D., and M. Yanai, 1989: Effects of downdrafts and mesoscale convective organization on the heat and moisture budgets of tropical cloud clusters. Part III: Effects of mesoscale convective organization. *J. Atmos. Sci.,* **46,** 1566–1588.

Cotton, W. R., H. Jiang, S. C. R. Rafkin, G. D. Alexander, and R. L. McAnelly, 1996: Parametrization of cumulus and MCSs in GCMs to mesoscale models. *Proc. ECMWF Workshop on New Insights and Approaches to Convective Parametrization,* Reading, United Kingdom, European Centre for Medium-Range Weather Forecasts, 288–305.

Donner, L. J., 1993: A cumulus parameterization including mass fluxes, vertical momentum dynamics, and mesoscale effects. *J. Atmos. Sci.,* **50,** 889–906.

——, C. J. Seman, and R. S. Hemler, 1999: Three-dimensional cloud-system modeling of GATE convection. *J. Atmos. Sci.,* **56,** 1885–1912.

Edwards, J. M., and A. Slingo, 1996: Studies with a flexible new radiation code. Part I. Choosing a configuration for a large-scale model. *Quart. J. Roy. Meteor. Soc.,* **122,** 689–719.

Fritsch, J. M., R. J. Kane, and C. R. Chelius, 1986: The contribution of mesoscale convective weather systems to the warm-season precipitation in the United States. *J. Climate Appl. Meteor.,* **25,** 1333–1345.

Gregory, D., and P. Rowntree, 1990: A mass flux convection scheme with representation of cloud ensemble characteristics and stability-dependent closure. *Mon. Wea. Rev.,* **118,** 1483–1506.

——, R. Kershaw, and P. M. Inness, 1997: Parametrization of momentum transports by convection. II: Tests in single-column and general circulation models. *Quart. J. Roy. Meteor. Soc.,* **123,** 1153–1184.

Houze, R. A., 1973: A climatological study of vertical transport by precipitating cumuli. *J. Atmos. Sci.,* **30,** 1112–1123.

——, 1977: Structure and dynamics of a tropical squall-line system. *Mon. Wea. Rev.,* **105,** 1540–1567.

——, 1989: Observed structure of mesoscale convective systems and implications for large-scale heating. *Quart. J. Roy. Meteor. Soc.,* **115,** 425–462.

——, 1993: *Cloud Dynamics.* International Geophysics Series, Vol. 53, Academic Press, 573 pp.

Johnson, R. H., 1984: Partitioning tropical heat and moisture budgets into cumulus and mesoscale components: Implications for cumulus parameterization. *Mon. Wea. Rev.,* **112,** 1590–1601.

Jorgensen, D. P., and M. A. Lemone, 1989: Vertical velocity characteristics of oceanic convection. *J. Atmos. Sci.,* **46,** 621–640.

Kershaw, R., and D. Gregory, 1997: Parametrization of momentum transport by convection. I: Theory and cloud modelling results. *Quart. J. Roy. Meteor. Soc.,* **123,** 1133–1151.

Leary, C. A., and R. A. Houze, 1980: The contribution of mesoscale motions to the mass and heat fluxes of an intense tropical convective system. *J. Atmos. Sci.,* **37,** 2444–2457.

Leonard, B. P., M. K. MacVean, and A. P. Lock, 1993: Positivity-preserving numerical schemes for multidimensional advection. NASA Tech. Memo. 106055 (ICOMP-93905), 62 pp.

Mason, P. J., 1989: Large-eddy simulation of the convective boundary layer. *J. Atmos. Sci.,* **46,** 1492–1516.

Moncrieff, M. W., 1992: Organized convective systems: Archetypal dynamical models, mass and momentum flux theory, and parametrization. *Quart. J. Roy. Meteor. Soc.,* **118,** 819–850.

——, S. K. Krueger, D. Gregory, J.-L. Redelsperger, and W.-K. Tao, 1997: GEWEX Cloud System Study (GCSS) Working Group 4: Precipitating convective cloud systems. *Bull. Amer. Meteor. Soc.,* **78,** 831–845

Piacsek, S. A., and G. P. Williams, 1970: Conservation properties of convection difference schemes. *J. Comput. Phys.,* **6,** 392–405.

Rickenbach, T. M., and S. A. Rutledge, 1998: Convection in TOGA COARE: Horizontal scale, morphology, and rainfall production. *J. Atmos. Sci.,* **55,** 2715–2729.

Rutledge, S. A., and R. A. Houze, 1987: A diagnostic modeling study of the trailing stratiform region of a midlatitude squall line. *J. Atmos. Sci.,* **44,** 2640–2656.

Shutts, G. J., and M. E. B. Gray, 1994: A numerical modelling study of the geostrophic adjustment process following deep convection. *Quart. J. Roy. Meteor. Soc.,* **120,** 1145–1178.

Smith, R. N. B., 1990: A scheme for predicting layer clouds and their water content in a general circulation model. *Quart. J. Roy. Meteor. Soc.,* **116,** 435–460.

Steiner, M., R. A. Houze, and S. E. Yuter, 1995: Climatological characterization of three-dimensional storm structure from operational radar and rain gauge data. *J. Appl. Meteor.,* **34,** 1978–2007.

Swann, H., 1998: Sensitivity to the representation of precipitating ice in CRM simulations of deep convection. *Atmos. Res.,* **47–48,** 415–435

Tao, W.-K., and J. Simpson, 1989: Modeling study of a tropical squall-type convective line. *J. Atmos. Sci.,* **46,** 177–202.

Thorpe, A. J., M. J. Miller, and M. W. Moncrieff, 1982: Two-dimensional convection in non-constant shear: A model of mid-latitude squall lines. *Quart. J. Roy. Meteor. Soc.,* **108,** 739–762.

Xu, K.-M., 1995: Partitioning mass, heat, and moisture budgets of explicitly simulated cumulus ensembles into convective and stratiform components. *J. Atmos. Sci.,* **52,** 551–573.

Yanai, M., S. Esbensen, and J.-H. Chu, 1973: Determination of bulk properties of tropical cloud clusters from large-scale heat and moisture budgets. *J. Atmos. Sci.,* **30,** 611–627.

Zipser, E. J., 1977: Mesoscale and convective-scale downdrafts as distinct components of squall-line structure. *Mon. Wea. Rev.,* **105,** 1568–1589.